The following article appeared in Arabian Journal of Chemistry 14(2): 102917 (2021) and may be found at: 10.1016/j.arabjc.2020.102917

Arabian Journal of Chemistry (2021) **14**, 102917

King Saud University

Arabian Journal of Chemistry

www.ksu.edu.sa
www.sciencedirect.com

ORIGINAL ARTICLE

Synthesis of keratine, silver, and flavonols nanocomposites *to* inhibit oxidative stress in pancreatic beta-cell (INS-1) and reduce intracellular reactive oxygen species production

Rosa Martha Pérez-Gutierrez [a,*], Isis Sherazada Rodríguez-Clavel [b], Silvia Patricia Paredes-Carrera [b], Jesus Carlos Sánchez-Ochoa [b], Alethia Muñiz-Ramirez [c], Susanna Medellin Garibay [d], Eri Joel Paz-García [b]

[a] *Laboratorio de Investigación de Productos Naturales, Escuela Superior de Ingenieria Quimica e Industrias extractivas, Instituto Politecnico Nacional, Av. Instituto Politécnico Nacional S/N, Unidad Profesional Adolfo Lopez Mateos cp 07708, Mexico, D.F, Mexico*
[b] *Laboratorio de Nanomateriales Sustentables. Sección de Estudios de Posgrado e Investigación - Escuela Superior de Ingeniería Química e Industrias Extractivas, Instituto Politécnico Nacional, Av. Instituto Politécnico Nacional S/N, Unidad Profesional Adolfo López Mateos, CP 07708 CDMX, Mexico*
[c] *CONACYT-IPICYT/CIIDZA, Camino a la Presa de San Jose 2055, Col. Lomas 4 sección, CP 78216 San Luis Potosí México, Mexico*
[d] *Laboratorio de Farmacia, Facultad de Ciencias Químicas, Universidad Autónoma de San Luis Potosí, Mexico*

Received 29 September 2020; accepted 29 November 2020
Available online 9 December 2020

KEYWORDS

Vaccinium macrocarpon;
Oxidative stress;
Flavonols;
Antioxidant enzymes;
Pancreatic β-cell

Abstract Flavonols (FLA) from *Vaccinium macrocarpon (V. macrocarpon*) were identified using high-performance liquid chromatography coupled with mass spectrometry detection. Nanoparticles were prepared using highly crosslinked keratin (KER) from human hair and silver and entrapped with flavonols [KER + FLA + AgNPs]. Nanocomposites were characterized using UV–Vis spectroscopy, transmission electron microscopy (TEM), X-ray diffraction, zeta potential, and dynamic light scattering, and release profiles. The interactions between the capping agent and the silver core have been investigated using FTIR spectroscopy·H_2O_2 is a source of Reactive Oxygen Species

* Corresponding author at: Laboratorio de Investigación de Productos Naturales, Escuela Superior de Ingenieria Quimica e Industrias extractivas, Instituto Politecnico Nacional, Av. Instituto Politécnico Nacional S/N, Unidad Profesional Adolfo Lopez Mateos cp 07708, Mexico, D.F., Mexico.
E-mail address: rmpg01@hotmail.com (R. Martha Pérez-Gutierrez).
Peer review under responsibility of King Saud University.

Production and hosting by Elsevier

https://doi.org/10.1016/j.arabjc.2020.102917

(ROS) and acts as an activator of oxidative stress affecting NS-1 cells, and the protective effect of the nanocomposites were evaluated against H_2O_2-induced pancreatic β-cell damage. LC-MS/MS and HPLC analyses revealed the presence of 12 flavonols in *V. macrocarpon* plant extract. The cell apoptosis and proliferation, were evaluated by Hoechst 33342 staining, flow cytometry and Cell Counting Kit-8 respectively. Preincubation of the NS-1 cells with 250 μg/mL of H_2O_2 induced oxidative stress conditions that show pancreatic β-cell dysfunction, including ROS, cell death, mitochondrial function, antioxidant enzymes, and lipid peroxidation. Nevertheless, pretreatment with FLA and [KER + FLA + AgNPs] prevented mitochondria disruption, maintained cellular ATP levels, inhibited LDH release, intracellular ROS production, decreased lipid peroxidation, increased expression of antioxidant enzymes (CAT, SOD, and GPx) and GSH levels. These results indicate that nanocomposites could protect rat INS-1 pancreatic β-cell from H_2O_2-induced oxidative damage, apoptosis and proliferation by reducing the production of intracellular reactive oxygen species.

1. Introduction

Reactive oxygen species generated in cells are an essential part of metabolism and aerobic life modulating various physiological functions in cellular signaling systems (Valko et al., 2007); excessive reactive oxygen species generation could cause damage to cells components, mainly mitochondrial dysfunction, which has been observed in pancreatic β-cells and several tissues in diabetic patients (Anello et al., 2005). Consequently, mitochondrial dysfunction induced by ROS may disrupt glucose-induced insulin secretion. The oxidative stress by an excessive generation of ROS disrupts the antioxidant defense system of the organism (Nikki, 2001).

In the pancreas, the islets of Langerhans have β-cell as the main cell type, which has a high sensitivity to oxidative stress produced mainly by a weak antioxidative defense system compared to other organs and tissues (Lenzen, 2008)·H_2O_2 is an intracellular messenger that can be degraded and synthesized quickly in response to external stimuli·H_2O_2 is generated in β-cells during glucose metabolism and used for glucose-stimulated insulin secretion as a metabolic signal (Pi et al., 2010). Elevated ROS levels inhibit insulin secretion leading to β-cell injury; as an alternative, when ROS levels are low, there is a release of insulin from β -cells. Consequently, the maintenance of redox balance is necessary to maintain β-cell functioning. An imbalance of H_2O_2 production and a low capacity for its inactivation is the principal cause of this deficiency (Gurgul-Convey et al., 2016).

Reactive oxygen species, such as hydrogen peroxide and superoxide, are mediators of oxidative stress formed mainly from electron leakage through oxidative phosphorylation. Utilizing glucose oxidase to deliver H_2O_2 continuously the β-cells can remove micromolar levels of this oxidant. In contrast, when delivered as a bolus, H_2O_2 decreases β-cell viability, depletes cellular energy stores, and damages DNA response. It is a common practice to utilize a single or repeated bolus of H_2O_2 when studying β-cell responses to the oxidants (Marinho et al., 2013); when delivered as a one-time bolus, H_2O_2 exhausts the antioxidant defenses of the cell, leading to the accumulation of depletion of intracellular energy stores, DNA damage, depletion and cell death (Stancill et al., 2019).

The formation and accumulation of ROS play an outstanding role in the complications of diabetes. Owing to the adverse effects of ROS on diabetic patients is essential to search for new drugs capable of reducing cellular oxidative stress to avoid pancreatic β -cell damage, to organize glucose homeostasis, and improve insulin secretion. The use of plant extracts has attracted attention from researchers in the last decades as a diabetic therapy due to the avoidance of side effects.

In recent years, nanoparticles (NPs) have had an essential application in the nanomedicine field (Suman et al., 2013); owing to their large surface area, small size, and unique properties like coating formulations (Templeton et al., 2000). Besides, the synthesis process of nanoparticles does not employ extreme conditions or toxic chemicals (Wang et al., 2018). Due to their high availability and biocompatibility, natural biopolymers have drawn increasing attention as drug delivery vehicles. Natural biopolymers for its biodegradability do not accumulate in organs like other materials, such as metal nanoparticles (Nel, 2006). Proteins are preferred among natural polymers for the loading and delivering of drugs; this is due to their structural characteristics, such as different pH values, which could have negative or positive charges above or below their isoelectric points.

Consequently, this can facilitate the attraction of hydrophobic molecules as water-insoluble drugs. Keratin is the main component of hair, horns, wool, nails, feathers, and other epithelial coverings (Li et al., 2017). Its use in the preparation of nanoparticles has several advantages over other nanostructures, such as the cost, which is less in extraction and purification than other proteins. The high content of cysteine residues in keratin is more appropriate to stabilize metals like Ag, producing keratin-capped nanoparticles (NPs), which can easily be transferred to organisms for biomedical applications because of their biodegradability and biocompatibility. The alpha helix is the main structural unit in keratin that can generate the capping agent with silver acting as stabilizers.

The basic side-chain of amino acids can play a crosslinking factor for pairs of particles (Zhong et al., 2004). It has been established that amino acid residues can stabilize silver nanoparticles (Tamerler et al., 2006).

Edible plants, known to be non-toxic, have been employed for the treatment of diabetes. Cranberry (*V. macrocarpon*) is a popular fruit cultivated worldwide due to its significant economic importance in many countries. Besides, cranberry has been used for centuries as a medicinal herb to treat several

human diseases. Studies have shown that cranberry has a wide range of pharmacological effects on the disease because of its antioxidant capacity (Drózdz et al., 2017). However, cytoprotective activity in pancreatic β-cells remains to be elucidated. Cranberry can control urinary tract infections due to the content of flavonoids as an alternative to the emerging antibiotic resistance (Howell et al., 2010). Besides, phenolic compounds avoid oxidative stress and chronic inflammation, among others (Skarpańska et al., 2017). Cranberry extract reduces visceral obesity and weight gain (Peixoto et al., 2017), ameliorates hyperglycemia, insulin resistance, and improves plasma lipid profile (Stefanescu, 2018). In another study, extract from blueberries (*Vaccinium* spp.) has been previously reported that could reverse the formation of AGEs (Ferrier et al., 2012); however, it has been reported that B-type procyanidin in *V. macrocarpon* causes the same effect (Sun et al., 2016). Previous studies have demonstrated that *V. macrocarpon* fruits ameliorate oxidative stress in H9c2 cardiomyocytes by suppressing the intracellular reactive oxygen species production (Brown et al., 2012).

On this basis, we describe 12 chemical constituents of *V. macrocarpon* and also the synthesis, characterization, and biocompatibility of nanocomposites [KER + FLA + AgNPs]. Besides, we investigate their protective effects on pancreatic β-cells (INS-1) exposed to H_2O_2 induced oxidative stress conditions in vitro experiments to obtain more information about their mechanism.

2. Materials and method

General High-performance liquid chromatography coupled to mass spectrometry detection was performed in an Agilent 6210, Time of Flight (TOF) (LC-MS, Ontario, Canada), The Fourier Transform Infrared (FTIR) spectra were measured on an Elmer 1650 FTIR spectrophotometer (Walthman, MA, USA). The UV–visible absorption was recorded using Shimadzu UV–visible spectrophotometer (UV-1650PC-Tokyo, Japan). The ζ potential, sizes as well as the hydrodynamic diameter of [KER + FLA + AgNPs] were evaluated using Delsa Nano C particle analyzer (Beckman Coulter, Inc., Brea, CA, USA). Size distributions were measured using a UTHSCSA Image Tool version 3.00 software. Nanoparticle dispersion was studied using a scanning electron microscopy (SEM), Hitachi S-4800 SEM (Hitachi, Inc., Tokyo, Japan). The crystallinity study of α keratin was evaluated using X-ray diffraction (XRD). A Rigaku SmartLab X-ray diffractometer with Bragg − Brentano *para*-focusing geometry was used. Diffraction intensities were recorded with 2θ ranging from 3° to 40°. All reagents and solvents were obtained from Sigma-Aldrich (St. Louis M, USA). Fluorescence was measured on a microplate reader (Thermo Fisher Scientific, FL, USA).

2.1. Plant preparation

Fresh *V. macrocarpon* fruit was collected from the Mexico State. The specimen was identified and authenticated by the specialist Biologist Aurora Chamal, from the Department of Botany, National School of Biological Sciences, National Polytechnic Institute, where a voucher specimen (No. 8945) has been deposited for further reference.

2.2. Plant extraction

Fresh *V. macrocarpon* was dried and grounded into a powder, then the powder (500 g) was extracted with 80:20 acetone/water (1 L × 3 times) for 4 h. The extract was concentrated and dried in a vacuum rotavapor, which was defatted by extraction with hexane (0.5 L) and was finally extracted with four portions of ethyl acetate (0.5 L; 20.6 g).

2.3. Analysis by HPLC

Ethyl acetate was loaded on an HPLC at 350 nm in a Develosil diol column (250 × 4.6 mm i.d., 5 μm; Phenomenex, Torrance, CA, USA). The mobile phase is composed of a binary gradient of (A) 2% formic acid and (B) 2% formic acid in methanol. The flow rate was 0.9 mL/min with the linear gradient: 10–30% B from 0 to 5 min; 25–40%B from 5 to 25 min; with 40% B from 25 to 30 min; 40–95% B from 30 to 45 min; and 95% B from 45 to 50 min; The column was equilibrated again with 0% B for 5 min. A PDA detector from 220 to 650 nm was used to monitor elution (Jin et al., 2016). For the identification of flavonols, standard curves were made using standards with a concentration of 1 mg/mL dissolved in methanol.

2.4. Extraction of Keratine

Human hair used for the experiment was obtained from a local barbershop, cut into small pieces, and washed with sodium hypochlorite solution at room temperature (25 °C) to remove pathogens, and dried at 40 °C for 6 h. The cleaned hair was hydrolyzed using a mix of H_2O-H_2SO_4 (1:1 v/v) stirring for 12 h at 50 °C, and the pH was adjusted between 4,0.5 (isoelectric point of keratin) with a 5 M sodium hydroxide solution. The mixture was precipitated, left for 24 h at room temperature, and treated by centrifugation at 15,000 rpm for 30 min. The precipitate was dissolved in 140 mL of ethanol–water and was dialyzed (6000–8000 Da MWCO Spectrapor dialysis) with four water changes over a 12-h period. The solution was irradiated with ultrasound (ultrasonic bath brand Elma D-78224, Elma ultrasonic, MIN, USA) at 3.8 kW and 45 kHz for 90 min. The solution was cooled to 4 °C until obtaining the crystallized phase and then was dried at 50 °C and turned to powder (Martin et al., 2011).

2.5. Coating of Keratin, silver nanoparticles and FLA

A solution of 50 mL of water and 0.184 g of $AgNO_3$ in a 250 mL Erlenmeyer flask was mixed in a rotary shaker at 120 rpm at room temperature for 1 h. Ag NPs were synthesized in dark conditions adding a solution of $NaBH_4$ to $AgNO_3$ in a molar ratio of 3:1 ($NaBH_4$/$AgNO_3$) with a constant stirring for 24 h. The reduction of $AgNO_3$ in silver nanoparticles was measured with a UV–visible spectrophotometer. The pH of the keratin solution was changed from 5.5 to 8.4–8.8, with the addition of keratin. Sodium hydroxide was added to obtain a pH in the range of 8.4–8.8. When all of the keratin was completely dissolved, and then Ag NPs are added, keeping the molar ratio 1:20 (keratin/$AgNO_3$) while varying the pH of the keratin/$AgNO_3$ solution (pH 9). The solution was treated

to remove unbound keratin and excess salts by dialysis with water for 24 h. The dialyzed solution was centrifugated at 12,000 rpm for 30 min. The [KER + AgNPs] solution without unbound keratin and salts was added to a FLA solution (90 mg/50 mL) with constant stirring for 48 h. Then [KER + FLA + AgNPs] was centrifugated at 15,000 rpm for 20 min (Vvedenskaya et al., 2004).

2.6. [KER + FLA + AgNPs] characterization

The Fourier Transform Infrared (FTIR) spectra were measured from 600 to 4000 cm^{-1}. The UV–visible absorption was recorded over the range of 300 to 800 nm. The ζ potential, size distributions, nanoparticle dispersion, the crystallinity study of keratin, diffraction intensities, geometry as well as the hydrodynamic diameter of [KER + FLA + AgNPs] were evaluated.

2.7. Stability of the nanocomposites

The stability in physiological conditions was evaluated. 500 mg of nanocomposites were suspended in 5 mL of phosphate-buffered saline (PBS) and maintained at 37 °C. The shelf life of the nanocomposites was recorded in pre-determined time intervals using absorbance intensities of the solutions over 6 months.

2.8. Entrapment efficiency (EE%) of nanocomposites

The nanocomposites suspension was centrifuged at 5000 rpm for 50 min. Then 1 mL of supernatant was added to 10 mL distilled water, and the absorbance was measured at 277 nm using water as blank. The content of the drug entrapped was measured by subtracting the amount of free drug in the supernatant from the initial amount of nanocomposites taken. The assay was tested in triplicate, and the average was calculated (Wang et al., 2011).

2.9. Release study

The release profiles of [KER + FLA + AgNPs] were determined using dialysis diffusion (MWCO 3.5 kDa) at 37 °C. 50 mg of [KER + FLA + AgNPs] was suspended in 5 mL of distilled water and transferred to a dialysis bag with phosphate buffer solution (pH 2.1) or phosphate buffer solution (pH 6.8) under a gentle stirring at 37 °C. In pre-determined time intervals, 4 mL of release media was taken, and then 4 mL of fresh media was added to the system. The amount of [KER + FLA + AgNPs] released in the medium was measured by UV/Vis spectrometer with a wavelength of 285 nm using calibration curves.

2.10. DPPH radical scavenging activity

The effects of the extract from *V. macrocarpon*, [KER + AgNPs] and [KER + FLA + AgNPs] on DPPH radicals was evaluated according to the Blois test (Blois, 1960). The three samples were dissolved in ethanol in a concentration range of 10 to 500 μg/ml. Then a solution of DPPH (600 μl) was mixed with 400 μl each of the samples and incubated for 30 min. The absorbance of the resulting solution was determined at 520 nm.

2.11. Determination of cell viability, lactate dehydrogenase and mitochondrial function

Rat pancreatic β cells (INS-1 cells) were purchased from the American Type Culture Collection (Manassas, VA, USA), and were maintained in an RPMI1640 medium (2 g/L glucose) 1% penicillin/streptomycin solution and supplemented with 10% fetal bovine serum (FBS). Cells were incubated with 95% air and 5% CO_2 at 37 °C.

To evaluate the protective effects of the FLA, [KER + AgNPs] and [KER + FLA + AgNPs] against H_2O_2-induced cell death, the incubation of INS-1 cells was performed with 10, 20, 50, 100, 200, 300, 400 and 500 μg/mL of skin keloid fibroblasts (KFS) for 20 h, before the addition of 0.7 mM H_2O_2 for 4 h. Cell viability was evaluated using the test 3-(4,5-dimethylthiazol-2-yl)-2,5-diphenyltetrazolium bromide (MTT; Sigma-Aldrich Co., St. Louis, MO, USA). Thus, oxidative stress was induced by the addition of 250 μM H_2O_2 for 4 h (Duan et al., 2015). The absorbance was measured at 570 nm.

Cell integrity was measured by LDH assay, determined as lactate dehydrogenase released in the culture medium (Duan et al., 2015). Briefly, INS-1 cells were incubated with 5, 10, 20 μg/mL of KFS, and [KER + AgNPs; 20 μg/mL] and 250 μM of H_2O_2 for 15 min, and after treatment, 0.2 mL culture medium of each group was evaluated for LDH activity using a commercial kit (Cayman Chemical, MI, USA).

Mitochondrial function was measured by cellular ATP analysis. KFS (5, 10 20 μg/mL) and [KER + AgNPs; 20 μg/mL] were added to the culture medium and maintained for 24 h before cellular ATP analysis·H_2O_2 250 mM was incorporated 2 or 4 h before the end of the experiment (Liang, et al., 2017). Cellular ATP levels were then measured in both cells exposed to KFS, [KER + AgNPs; 20 μg/mL], and H_2O_2 250 mM using a fluorometric assay kit (Abcam, Boston, MA, USA) according to the manufacturer's instruction.

2.12. Evaluation of intracellular ROS with stimulation of H_2O_2

1 × 105 INS-1 cells per well in 96-well plates were pretreated for 24 h with KFS (5, 10, and 20 μg/mL) and 20 μg/mL of [KER + AgNPs] followed by addition of 250 μM H_2O_2; a reference was prepared without pretreated using 250 μM H_2O_2. After 24 h, the cells were reacted with 1 μM 2′,7′-Dichlorofluor escin diacetate (DCFH-DA, Sigma-Aldrich, St Louis MI, USA), at 37 °C for 30 min (Xu et al.,2013). Fluorescence was measured at 485 nm of excitation and 527 nm of emission wavelengths on a microplate reader.

2.13. Lipid peroxidation in INS-1 cell lines

Lipid peroxidation was measured with a thiobarbituric acid reactive substance (TBA-RS) using a Cayman TBA-RS assay kit (Cayman Chemical, Ann Arbor, MI, USA) according to the manufacturer's instructions (Yagi, 1998). The lipid peroxide generated from polyunsaturated fatty acids was decomposed in a complex series of compounds such as reactive carbonyl species, including malondialdehyde (MDA), which

is used to evaluate lipid peroxidation at an absorbance of 532 nm. The results are in μmol/μg protein.

2.14. Antioxidant enzymes and reduced glutathione

INS-1 cells seeded with a density of 5 × 105 cells/well were grown in RPMI-1640 for 24 h. Then, the medium was replaced with KFS (5, 10 20 μg/mL) and [KER + AgNPs; 20 μg/mL] in the presence of 250 μM of the prooxidant agent (H_2O_2). GSH, GPx, CAT, and SOD activities were performed according to the manufacturer's instruction (Cayman Chemical Company assays Kit, Michigan, USA). The activity is in mg protein for all antioxidant enzymes.

2.15. Hoechst 33,342 staining

Apoptosis in INS-1 cell was measured via Hoechst 33,342 staining. Then pre-incubation with nanocomposites at concentration of 25.0 μmol/L for 1 h and after of the exposure to 0.3 mmol/L H_2O_2 for 3 h, the cells were fixed in 4% paraformaldehyde and stained with 10 μg/mL Hoechst 33342. In a fluorescence microscopy (JXI500FL, Western Electric & Scientific Works, India), the photos were obtained and the apoptosis ratio in each group was evaluated.

2.16. Analysis of apoptosis by flow cytometry

The INS-1 cells were seeded at 3×10^5 cells/well in conditioned RPMI medium. After cells were harvested then incubating for 72 h, with H_2O_2 (0.3 mmol/L) or nanocomposites (25.0 μmol/L), non treated cells were used as controls, later using in cold phosphate buffered saline (PBS) were washed and resuspended, To detect INS-1 cell apoptosis was used an apoptosis Kit (Thermo Fisher Scientific, USA) according to the manufacturer's protocol. The cells in the wells were stained with FITC-conjugated annexin-V and Annexin-V/propidium iodide (PI) for 15 min at room temperature, and the apoptotic rates were evaluated by a flow cytometer (2020 Attune NxT Flow Cytometer, Thermo Fisher Scientific, USA).

2.17. Cell proliferation assay

The INS-1 cell proliferation was determined by using the Cell Counting Kit-8 (CCK-8) (MedChem Express, USA). The cells were seeded at concentration of 2×10^4 cells/well in RPMI conditioned medium. After 24 h of exposure to H_2O_2 (0.3 mmol/L), the cells were treated with NC (25.0 μmol/L) and non-treatment cells were used as control (Control). Then 10 μl of CCK-8 solution was added to each well previously incubation. Then, the cells were incubated for 72 h. The proliferation of the cells was measuring at an absorbance of 450 nm using a microplate reader. The amount of cell proliferation in each group was indicated as a percentage against the 2×10^4 cells.

2.18. Statistical analysis

The data are expressed as the mean ± SEM. The results were evaluated by one-way ANOVA, followed by Tukey's multiple comparison tests. The values of $p < 0.05$ were considered statistically significant.

3. Results and discussion

3.1. Compounds in V. macrocarpon

Flavonols compounds in *V.macrocarpon* fraction were identified by HPLC. Data analyses show more than 12 peaks found at the absorbance of 285 nm (Fig. 1). Flavonols were identified by comparison with UV spectra and their retention time data with the standards as follows: (**1**) Cyanidin-3-O- galactoside; (**2**) Cyanidin −3-O-arabinoside; (**3**) Peonidin-3-O-galactoside; (**4**) Kaemperol 3-O-glucoside; (**5**) Cyanidin-3-O-glucoside; (**6**) Peonidin −3-O-arabinoside (**7**) Quercetin-3-O-glucoside; (**8**) Quercetin-3-O-arabinoside; (**9**) Quercetin-3-O.rhamnoside; (**10**) Peonidin-3-O-glucoside; (**11**) Kaemperol 3-O-galactoside; (**12**) Kaemperol (Fig. 2). The identities of **1**–**12** were performed by comparing spectroscopic data to those previously published (Vvedenskaya et al., 2004). The compounds with greater proportion and with stronger antioxidant activity were the following flavonols: Peonidin-3-O-galactoside, Kaemperol 3-O-galactoside, Quercetin-3-O- arabinoside and Cyanidin-3-O- glucoside (Zheng and Wang, 2003; Liu et al., 2015; Zhu et al., 2015; Zucca et al., 2013).

3.2. Keratin characterization

Fig. 3A shows the X-ray analysis from human hair keratin. Keratin exhibited the crystallographic reflections for alpha keratin at (331), (040) and beta keratin at (111), (200), (020), (220), (400); the beta structure predominates in the material with crystalline spacings at 4.4 and 9.8 Å. As a complement of the keratin presence, we have the FTIR spectrum (Fig. 3B) that shows peptide bonds present in the keratin structure such as amide I, II and III. The band at $\nu = 3300\ cm^{-1}$ corresponds to amide I, at $\nu = 1560\ cm^{-1}$ to amide II, and $\nu = 1250–1270\ cm^{-1}$ to amide III.

3.3. [KER + FLA + AgNPs] characterization

The color of the solution of $AgNO_3$ changed from clear transparent to grizzly after the addition of $NaBH_4$, evidencing the formation of AgNPs. There is no variation in color during the next 3 days, indicating that the incubation time and particle generation have ended. As indicated in Fig. 4A (KER + FLA + AgNPs), the surface plasmon resonance absorption of the AgNPs is observed at 403 nm in the UV–visible spectra (Martin et al., 2011). Whereas, flavonols fraction is shown as an intense absorption peak at 280 nm (Fig. 4A).

FTIR spectrum of keratin (Fig. 4B, KER) shows bands at 1650 cm^{-1} and 1580 cm^{-1} attributed to amide I (C = O stretch), and amide II (C-N stretch) resplectively. The band at 1220 cm^{-1} corresponds to the in-phase combination of the C-N stretch vibrations (amide III) and N-H bending (Li et al., 2017). FTIR spectrum of flavonols fraction (Fig. 4B, FLA) indicated the presence of a hydroxy group at 3400 cm^{-1}, an aromatic group at 1650 cm^{-1}, carbonyl functionality at 1700 cm^{-1}, other bands at 1400 cm^{-1}, 1205 cm^{-1}, and 1100 cm^{-1}. The composites (Fig. 4B, KER + FLA + AgNPs) show characteristic bands of their components, such as 1700 cm^{-1}, 1650 cm^{-1}, 1580 cm^{-1}, and 1220 cm^{-1} of KER and FLA. In nanocomposites, the keratin surface absorbs AgNPs; amide groups form bonds with Ag

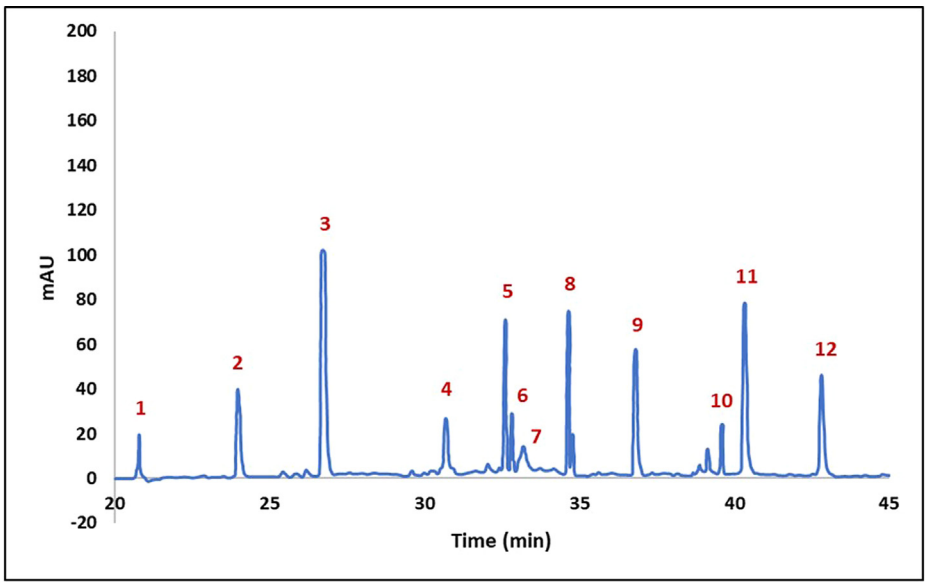

Fig. 1 Chromatograms obtained by HPLC analysis of an extract rich in flavonols from *Vaccinium macrocarpon:* (**1**) Cyanidin-3-O-galactoside; (**2**) Cyanidin −3-O-arabinoside; (**3**) Peonidin −3-O-galactoside; (**4**) Kaemperol 3-O-glucoside; (**5**) Cyanidin-3-O- glucoside; (**6**) Peonidin −3-O-arabinoside (**7**) Quercetin- 3-O-glucoside; (**8**) Quercetin-3-O- arabinoside; (**9**) Quercetin-3-O.rhamnoside; (**10**) Peonidin-3-O-glucoside; (**11**) Kaemperol 3-O-galactoside; (**12**) Kaemperol.

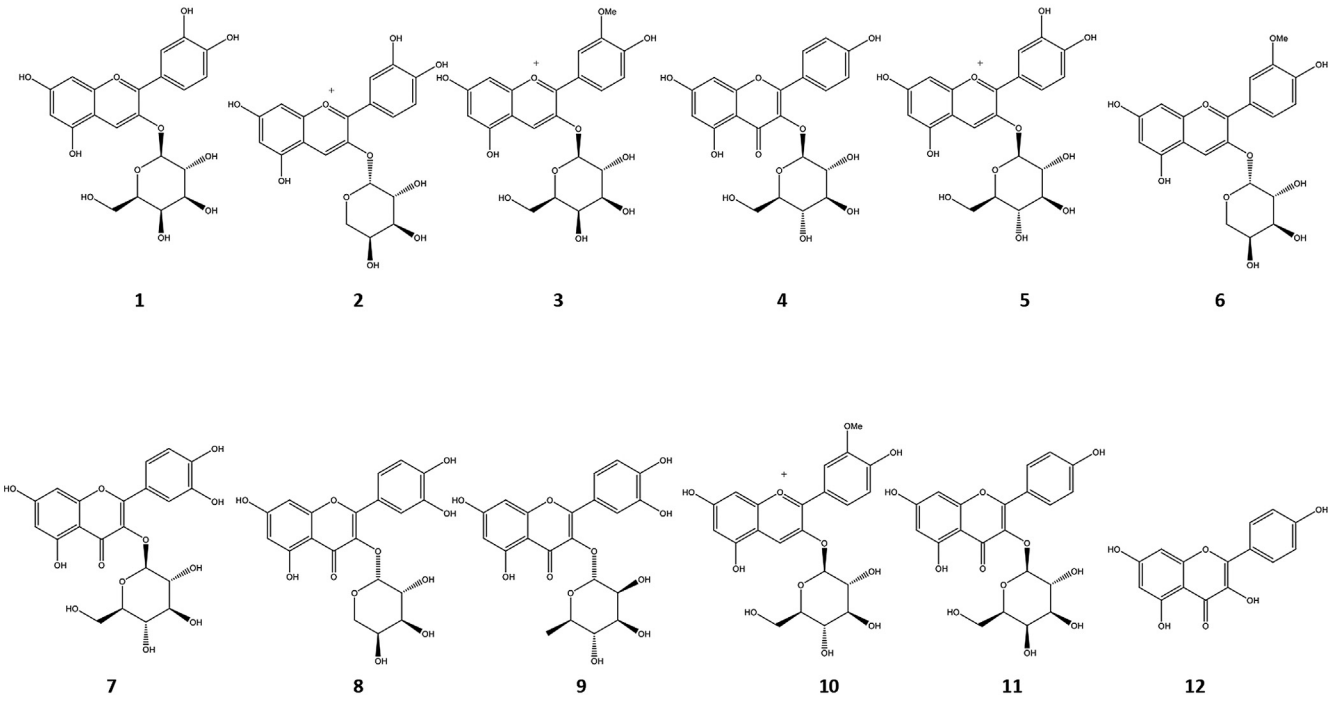

Fig. 2 Molecular structure of compounds.

atoms, changing the N–H band. Consequently, keratin forms a coating layer over silver nanoparticles stabilizing the NPs (Zhang et al., 2015).

3.4. Morphologies, diameter, polydispersity and entrapment efficiency (EE%) of nanocomposites

Keratin stabilizer strongly interacts with the silver ions, and this is supported by the FTIR spectrum; additionally, keratin free functional groups can quickly adsorb fragmented silver nanoclusters. KER includes a considerable quantity of chemically reactive $–NH_2$ and its free amino groups, which can react with silver and ^{-}OH groups of flavonoids to produce a cross-linked polymeric network. The morphology of [KER + FL A + AgNPs] nanocomposites have been examined by SEM (Fig. 5A). These nanocomposites are well dispersed, with minimal agglomeration forming small and spherical particles, and there is no tendency to agglomerate. The results obtained from

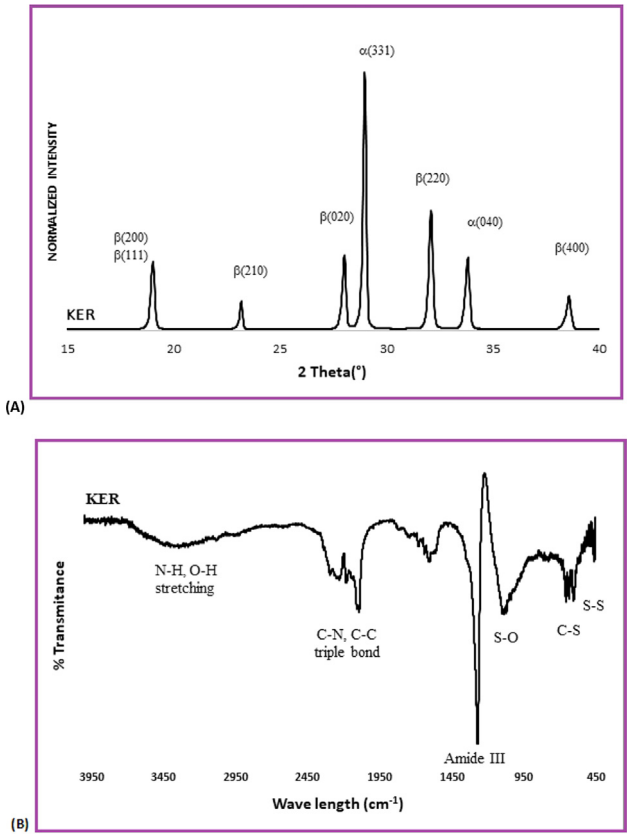

Fig. 3 (**A**) XRD spectrogram of keratin from human hairs (KER); (**B**) FTIR analysis of KER.

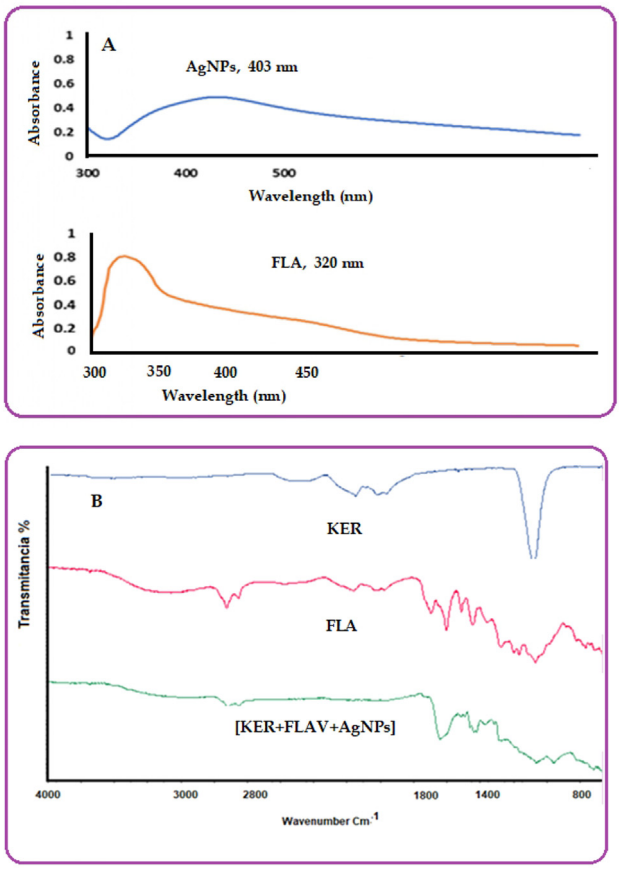

Fig. 4 (A) UV–vis spectra of AgNPs and FLA; (B) FT-IR spectra for keratin, FlA and nanocomposites [KER + FLA + AgNPs].

DLS showed that [KER + FLA + AgNPs] NPs sizes are in the range of 18–65 nm (Fig. 5B), suggesting that the nanocomposites can be suitable for medical applications. The average diameter of nanoparticles of ~35 nm ± 0.58 nm, as shown in Fig. 5B. Further examination indicated that the apparent zeta potential was −21.9 ± 0.3 mV, and particle polydispersity (PDI) was 0.424 ev (Fig. 5C). Entrapment efficiency (EE%) of nanocomposites of FLA in [KER + FLA + AgNPs] was 83%.

3.5. Stability of nanocomposites

Silver plasmonic band at 403 nm was studied for changes over three months. The surface plasmon peak was observed over the study period, and no noticeable changes were recorded, suggesting near monodispersed nanoclusters of silver capped in keratin. Consequently, the synthesis of nanocomposites was satisfactory.

3.6. Profile of drug-loaded

The release behavior of FLA from the nanocomposites was studied and compared in simulated gastric and intestinal fluids. The release percentage of FLA in both pH from the nanocomposites are shown as a function of time in Fig. 5D. The finding indicates that only a small amount of FLA is released from the matrices of nanocomposites in simulated gastric fluid due to poor solubility of FLA in the acidic medium. Nonetheless, nanocomposites after being added to the simulated intestinal fluid, it is was observed that the release rate at the beginning was higher as a consequence of the dissolution of surface-adhered FLA, and thus, the FLA release rate was delayed owing to the diffusion course of FLA from the internal network to the external solution.

3.7. DPPH radical scavenging activity of FLA, [KER + AgNPs], and [KER + FLA + AgNPs]

To measure the radical scavenging activity of the FLA, [KER + AgNPs], and [KER + FLA + AgNPs], we determine their effects in absence and presence on scavenging diphenylpicrylhydrazyl (DPPH) radicals. As shown in Fig. 6A, the [KER + AgNPs] did not show an antioxidant effect. However, FLA and [KER + FLA + AgNPs] in a dose-dependent manner, a 500 μg/ml dose in each sample induces inhibition of DPPH radicals between 64 and 72% respectively. [KER + FLA + AgNPs] exhibited the most potent DPPH radical scavenging activity, compared with FLA. These results indicated that FLA and [KER + FLA + AgNPs] have good antioxidant properties.

3.8. The viability of INS-1 pancreatic β-cells against oxidative stress induced by H_2O_2

To assess the toxicity with which FLA, [KER + AgNPs], and [KER + FLA + AgNPs] affect INS-1 β-cells viability, we

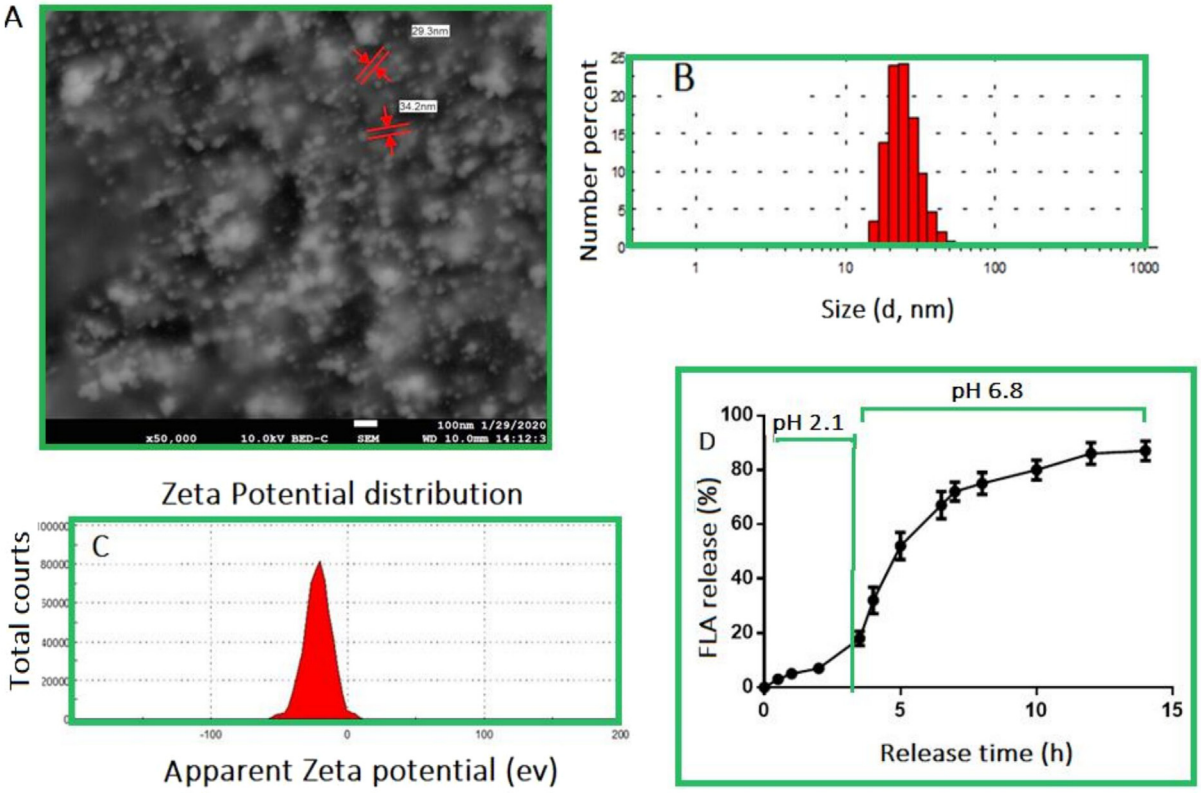

Fig. 5 (**A**) SEM micrograph showing the morphological characteristics of KER, silver nanocomposites bio-synthesized using the flavonols from *Vaccinium macrocarpon* fruits; (**B**) size distribution of [KER + FLA + AgNPs]; (**C**) zeta potential of nanocomposites; (**D**) release profiles of FLA in simulated gastric fluid (pH 2.1) and simulated intestinal fluid (6.8). Data represent the means ± SD of 3 independent experiments, $p < 0.05$, significantly difference.

employed the MTT assay (Fig. 6B). The cell viability was < 99% in the presence of all samples, up to a concentration of 10–500 µg/ml. However, in the case of [KER + AgNPs], cell viability at a 500 µg/ml dose was 88%.

The protective effects of FLA, [KER + AgNPs], and [KER + FLA + AgNPs] in the H_2O_2-treated INS-1 cells were measured by MTT assay. Exposition of INS-1 cells to H_2O_2 (250 µM) for 4 h derived in a significant cytotoxicity which was measured using MTT assay and LDH leakage test. The maximum inhibition in cell viability was observed at 49.1%, with the highest concentration of 250 µM H_2O_2 ($P < 0.05$ vs. control). Then, to evaluate the protective effect of FLA, [KER + AgNPs], and [KER + FLA + AgNPs] against H_2O_2-induced pancreatic cells damage, the cells were pretreated with various concentrations of FLA, [KER + AgNPs], and [KER + FLA + AgNPs] continued by addition of H_2O_2 for 4 h. In these experiments, the cell viability was restored to 70 and 85% when pretreated with 500 µg/ml of FLA and [KER + FLA + AgNPs], respectively, compared to the control sample (Fig. 6C). [KER + AgNPs] was particularly not effective in avoiding H_2O_2-induced cell death. Evidence indicates that H_2O_2 has an important participation in pancreatic-cell survival. In this study, we reported that [KER + FLA + AgNPs] promoted a change in the H_2O_2-activated cell death in β-cells to the apoptotic and necrotic pathway (Sun et al.,2012). Accordingly, FLA and [KER + FLA + AgNPs] are efficient at avoiding cell death induced by oxidative stress.

3.9 Effects on LDH production against H_2O_2-induced oxidative stress

LDH is an enzyme found widely in all tissues of the body and represents cell injury. The protective effect of FLA, [KER + AgNPs], and [KER + FLA + AgNPs] was also measured by detecting the LDH leakage produced by H_2O_2. When INS-1 cells were exposed for a period of 24 h to high H_2O_2 treatment cytotoxicity in a dose-dependent manner (data are not shown here), it is noted intense membrane damage with subsequent release of LDH. As shown in Fig. 7A, a 2.5 fold increase in LDH was observed in INS-1 cells treated with H_2O_2-induced oxidative stress compared to the control cells. However, [KER + AgNPs] at all concentrations tested did not show effects on LDH production. While [KER + FL A + AgNPs] pretreatment at 500 µg/mL significantly inhibits the increase of LDH levels in a dose-dependent manner, reducing LDH release 1.33 fold. We observed that [KER + FLA + AgNPs] treatment significantly inhibited the LDH enzyme release.

3.10. Nanocomposites attenuate H_2O_2-induced mitochondria function in INS-1 pancreatic β-cells

To evaluate the contribution of FLA, [KER + AgNPs], and nanocomposites in the maintenance of mitochondrial function of INS-1 pancreatic β-cells, we examined ATP in cells treated

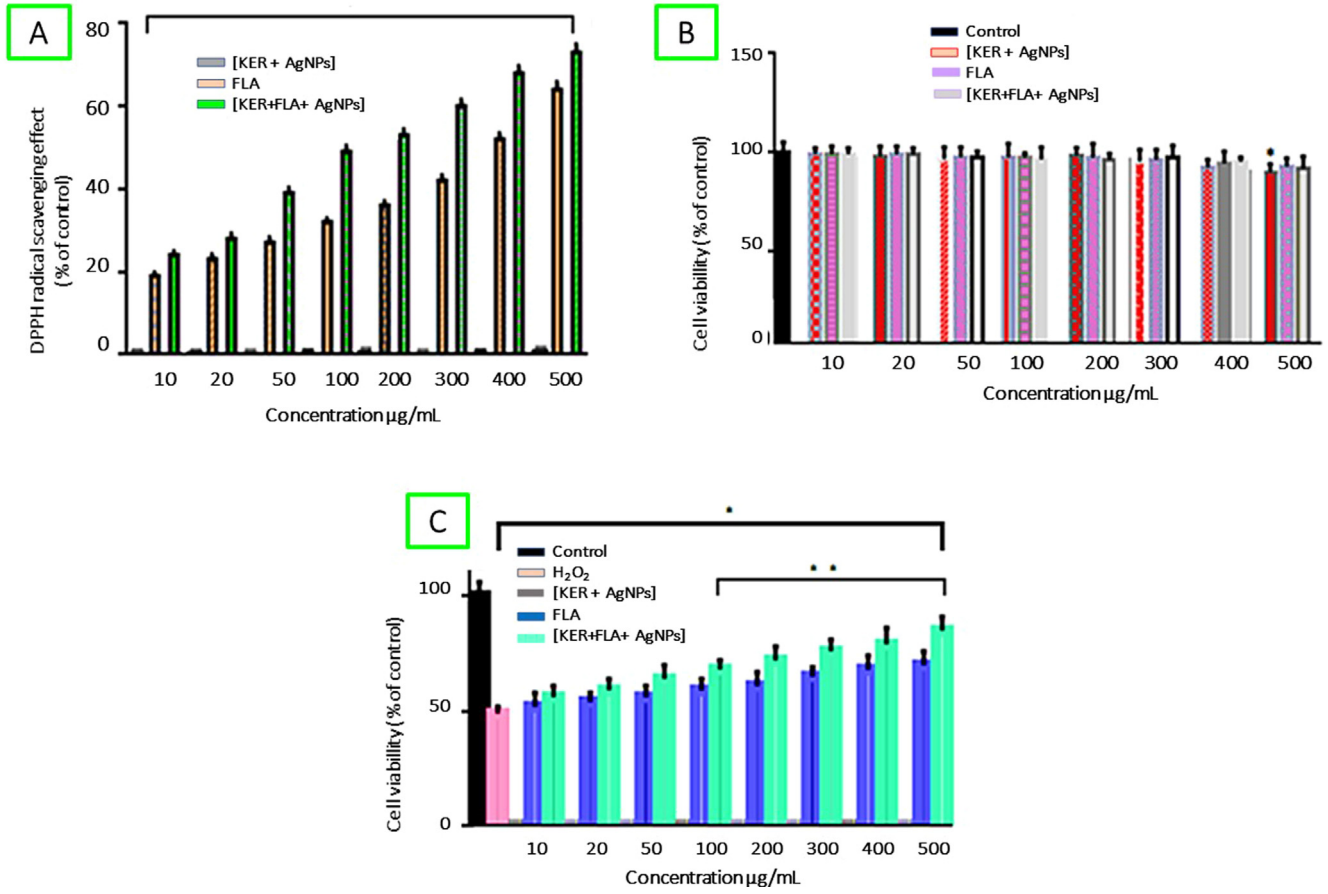

Fig. 6 (**A**) The amount of 2,2-Diphenyl-1-picrylhydrazyl (DPPH) radical scavenging activity was evaluated spectrophotometrically at 520 nm at a range of concentrations of 10–500 µg/ml; (**B**) Cell viability of pancreatic β-cells (INS-1 cells) treated with various concentrations of (10–500 µg/ml) of [KER + AgNPs], FLA and [KER + FLA + AgNPs] for 24 h, data causing < 70% viability are considered cytotoxic; (**C**) Protective effects of [KER + AgNPs], FLA and [KER + FLA + AgNPs] against oxidative stress-damaged pancreatic β-cells (NS-1). Data represent the means ± SD of 3 independent experiments. *$p < 0.01$ compared with untreated control cells; **$p < 0.05$, significantly difference compared with compared with cells treated with H_2O_2 only.

with H_2O_2. At the screening dose of 500 µmg/mL, [KER + AgNPs] has no effect on cells treated with H_2O_2. However, [KER + FLA + AgNPs] significantly increased in 2.28 fold ATP in cells (Fig. 7B, $p < 0.05$). In contrast, FLA at 500 µmg/mL significantly ($p < 0.05$) increased ATP formation in 1.68 fold (Fig. 7B, $p < 0.05$). [KER + FLA + AgNPs] restored mitochondrial function better than FLA. Pancreatic β-cell damage is related to the improvement of ROS generation and mitochondrial impairment. Mitochondrial dysfunction plays a vital role in the development of diabetes for its participation in controlling oxidative phosphorylation, ATP production, and electron transport; when those functions are disturbed, cell death may occur (Supale et al., 2012). β-cell mitochondria are the main site of ROS generation, and ROS loading carries to mitochondrial dysfunction and leakage through the mitochondrial external membrane. A reduction in ATP in cells is distinctive in the early apoptotic period (Supale., 2012). In this research, we have displayed that [KER + FLA + AgNPs] sustains mitochondrial function and reduce cellular ROS in the presence of H_2O_2. This could reduce oxidative damage and renovation of the function of β-cells suggesting the probability that mitochondria-targeted antioxidants can protect β-cells of cumulative damage impairment in type 2 diabetes.

3.11. Nanocomposites attenuate H_2O_2-induced ROS generation

The cellular oxygen metabolism generates ROS as by-products, which are used at low concentrations in cellular signaling. Thus, the increase of ROS usually produces significant free radical-mediated chain reactions targeting DNA, polysaccharides, lipids, and proteins (Slimen et al., 2014). It is known that H_2O_2-induced stress conditions generate elevated ROS levels in pancreatic β-cells (Aranda et al., 2013). Therefore, we have evaluated the role of FLA, [KER + AgNPs], and [KER + FLA + AgNPs] in ROS production during H_2O_2 induced stress conditions. It is shown in Fig. 7C, when the INS-1 cells were exposed to 250 µM of H_2O_2, there is an increase in the generation of ROS in 1.35 fold compared with the control group. Instead, pretreatment with nanocomposites (500 µg/mL) inhibited DCF fluorescence intensity in 1.31-fold, which is an indicator of ROS accumulation in a concentration-dependent manner in INS-1 cells compared to the control

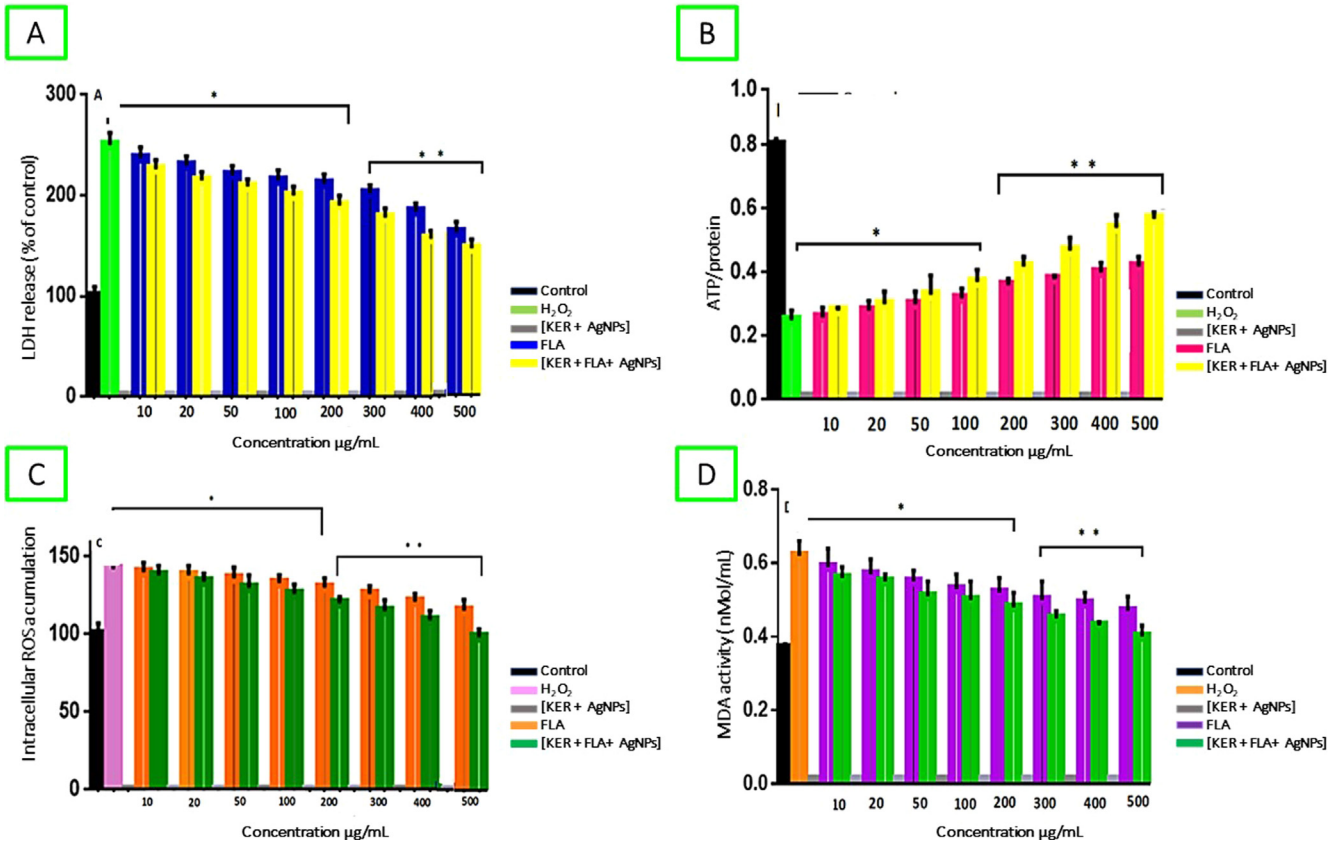

Fig. 7 Effect of [KER + AgNPs], FLA and [KER + FLA + AgNPs] on: (**A**) LDH release in H_2O_2–treated INS-1 cells; (**B**) ATP/protein (**C**) Intracellular ROS accumulation; (**D**) MDA activity . The data represent the mean of three independent experiments. *p < 0.01, compared with untreated control cells; **P < 0.01, compared with cells treated with H_2O_2 only.

group treated with H_2O_2. Data indicate high protection of H_2O_2 induced cell injury. Whereas pretreatment with 500 µg/mL of FLA decreased 1.16-fold ($p < 0.01$) in ROS accumulation compared with the control.

Results indicated that H_2O_2 treatment induces a reduction of ATP generation with a parallel increment in ROS levels as an early event in the apoptotic pathway leading to cell death (Aranda et al., 2013). In our studies, we observe that nanocomposites attenuate levels of ROS generation and maintain mitochondrial function in the INS-1 cells exposed oxidative stress improving β-cell function and destruction.

3.12. Thiobarbituric acid reactive species (TBA-RS) levels

Lipid peroxidation was determined by evaluating the level of malondialdehyde (MDA), which is considered as the end product of lipid peroxidation. Exposure to the INS-1 cells with H_2O_2 produced a significant ($p < 0.05$) 1.67 fold increase in MDA content compared to control cells (0.37 nM/mL). [KER + FLA + AgNPs] pretreatment produced a significant ($p < 0.05$) reduction (1.55 fold) in the MDA activity in the cells pretreated with 50 µg/mL, supporting that nanocomposite alleviated H_2O_2-induced lipid peroxidation (Fig. 7D). Whereas, FLA inhibits MDA activity in 1.44 fold at the same concentration.

Lipid peroxidation is the principal mechanism of free radical damage to membrane-bound enzymes and cellular organelles caused by mitochondrial ROS, which produced reactive aldehydes as cytotoxic products (Kappus, 1987). Therefore, lipid peroxidation can induce cell apoptosis, involved in numerous pathophysiological disorders (Jörns et al., 2016). Findings indicated that H_2O_2 treatment induced lipid peroxidation in pancreatic cells, and [KER + FLA + AgNPs] displays a significant reduction in TBA-RS production. Our studies observed that the nanocomposite has a significant reduction of mitochondrial ROS generation, consequently with a decreased level of lipid peroxidation under oxidative stress conditions. The protective effect of [KER + FLA + AgNPs] on TBA-RS generation can be attributed to its antiperoxidative effects.

3.13. Antioxidant enzymes in INS-1 pancreatic β-cells when treated in stress conditions

We used H_2O_2 toxicity in INS-1 cells as a model to measure the antioxidant defense system when treated with FLA, [KER + AgNPs], and [KER + FLA + AgNPs] previously exposed to H_2O_2. The improvement on neutralizing ROS oxidative stress was evaluated by assessing the levels of antioxidant enzymes such as (CAT), superoxide dismutase (SOD), glutathione peroxidase (GPx), and glutathione (GSH). H_2O_2-treatment causes a 1.44, 5.12, 1.52, and 1.77 fold decrease in CAT, SOD, GPx and GSH, respectively, when compared with control cell line. However, this reduction was prevented by FLA and [KER + FLA + AgNPs] pretreatment with a dose of 300 to 500 µg/mL ($p < 0.05$; Fig. 8(A-D)).

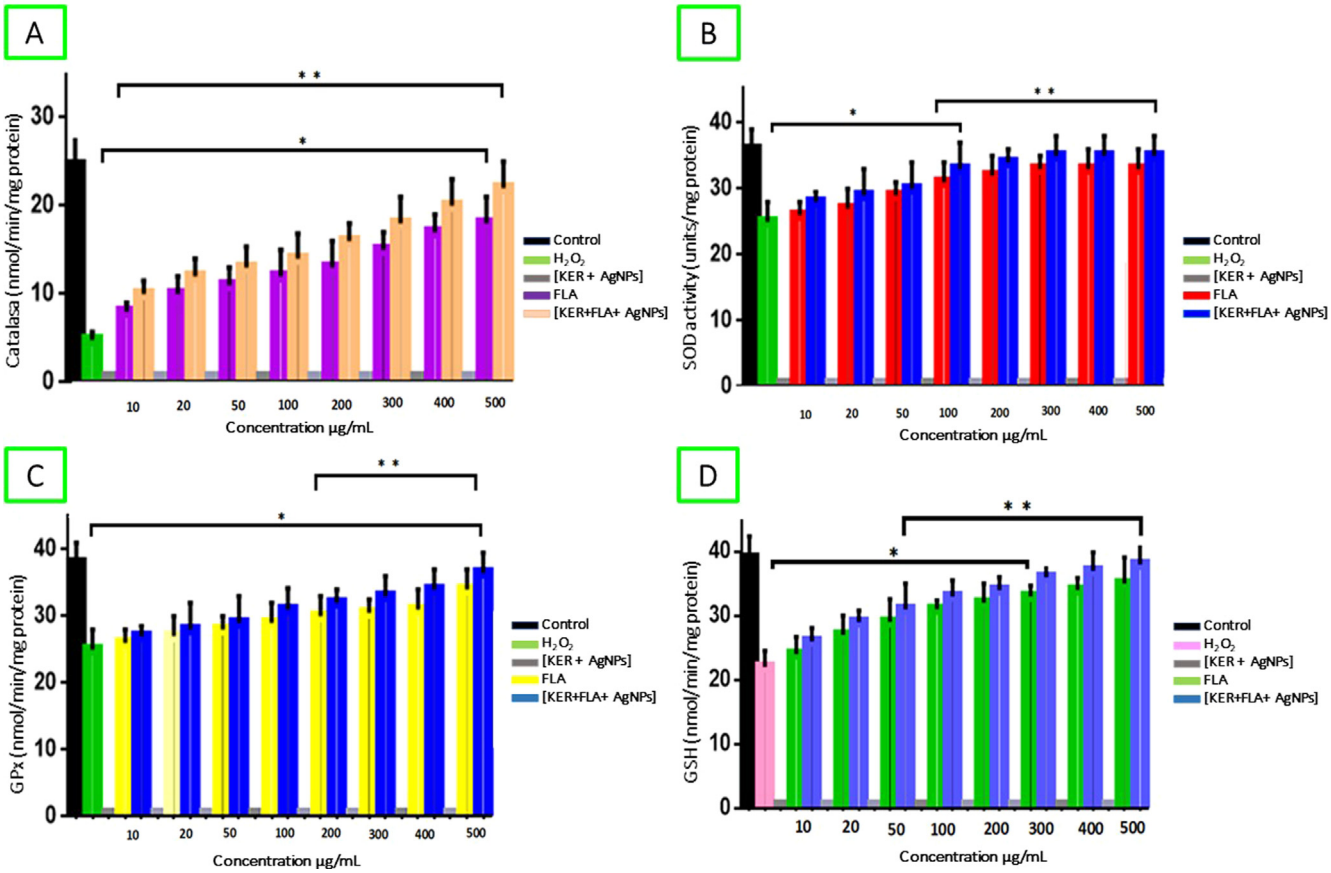

Fig. 8 Effect of [KER + AgNPs], FLA and [KER + FLA + AgNPs] on levels of antioxidant enzymes in H_2O_2-stress-induced in INS-1 pancreatic β-cells. (A) CAT; (B) CAT; (C) GPx and (D) GSH. data are presented as the mean ± standard (n = 3). *p < 0.01, compared with untreated control cells; **P < 0.01, compared with cells treated with H_2O_2 only.

Oxidative stress consequence from an imbalance between ROS formation and antioxidant defenses such as CAT, SOD, and GPx and the non-antioxidant enzyme (GSH) are the primary cellular antioxidant defenses (Shu, 1998) that can act together to decrease the ROS generated in β-pancreatic cells by H_2O_2 exposition. SOD catalyzes the transformation of superoxide anion ($O_2\cdot^-$) to H_2O_2 and molecular oxygen; then these are metabolized into molecular oxygen and water by GPx and CAT (Brown et al., 2012). The capacity and stability of the antioxidant enzymes against ROS during diabetes have an important role in the development of complications caused by ROS (Evans et al., 2002). The increase levels of antioxidant defenses stimulate cellular ability to scavenge free radicals, reducing the injury produced by ROS (Aouacheri et al., 2009). In our study treatment with FLA and [KER + FLA + AgNPs] an increased expression of CAT, SOD, GPx and GSH is observed, which was sufficient to counteract the oxidative stress induced by H_2O_2 protecting the β-cells which are susceptible and vulnerable to oxidative stress (Lyu et al., 2016).

3.14. Nanaocomposites protects INS-1 cells from H_2O_2-induced apoptosis

We also after examined the protective effects of KER + FL A + AgNPs, on the apoptosis induced by H_2O_2 in INS-1 cells. The apoptotic INS-1 cells were evaluated using Hoechst 33,342 staining. The fluorescent photomicrographs of the normal cells indicated an oval-shaped nuclei with homogeneous fluorescence, whereas in H_2O_2-induced INS-1 cells chromatin condensation and heterogeneous intensities were observed and the nuclei of apoptotic cells were measured for statistical assay. Finding, indicated that after the cells were exposed to H_2O_2, the percentage of apoptotic nuclear was 47.15% ± 14.24%; while, the percentages of apoptotic cells pretreated with the nanocomposites at 25.0 µmol/L was of 13.45% ± 7.21% (Fig. 9A). Results suggested that KER + FLA + AgNPs, protected INS-1 cells against H_2O_2-triggered injury exerted its protective activities partway reducing the apoptotic pathway and through the scavenging of ROS.

3.15. Measure of apoptosis by flow cytometry

The Annexin-V and Annexin-V/propidium iodide staining was performed to evaluate whether [KER + FLA + AgNPs] could enhance H_2O_2-induced apoptosis in INS-1 cells. The cell apoptosis rate in the H_2O_2 group was 43.0% (Fig. 9B), indicating that H_2O_2 exposition accelerated cell apoptosis. However, these results were significantly ($p < 0.05$) higher than in the group treated with nanocomposites with 19% of apoptosis. This finding suggests that [KER + FLA + AgNPs] can protect INS-1 cells reducing the apoptosis rate and oxidative stress of INS-1 cells during H_2O_2 treatment.

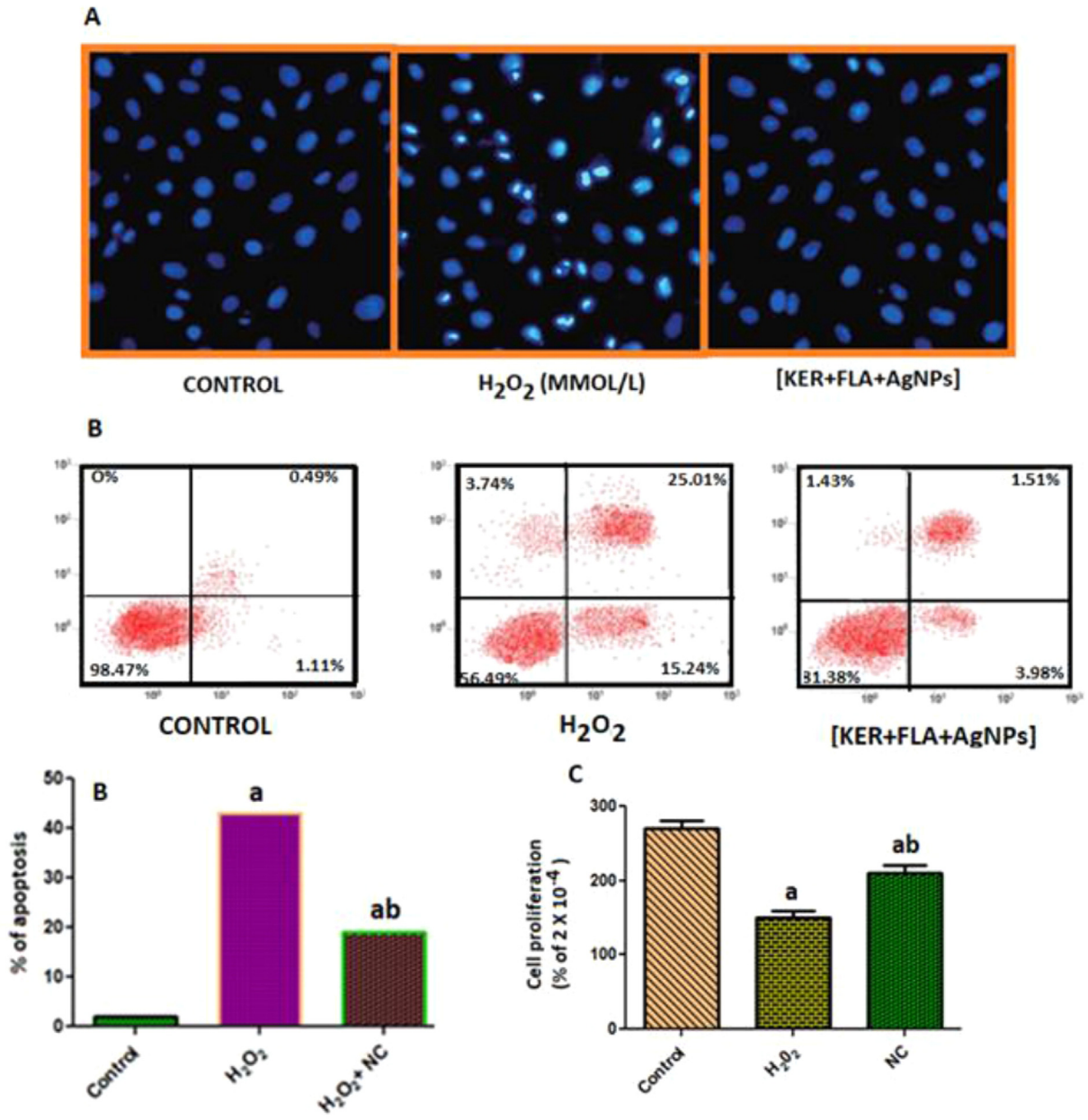

Fig. 9 (**A**) Control Is a typical fluorescent photomicrographs obtained with Hoechst 33,342 staining; However, in NS1 treated with H_2O_2 was observed the brighter nuclei indicated positive apoptotic cells in Hoechst 33,342 assay. Scar bar = 50 μm assign to three panels; (**B**) Protective effect of nanocomposites against H_2O_2 induced apoptosis; (**C**) Cell proliferation was evaluated by a CCK-8 assay. Results are representative of three different assays. $^{a}p < 0.05$ vs. Control, $^{b}p < 0.05$ vs·H_2O_2.

3.16. [KER + FLA + AgNPs] protects proliferation in INS-1 cells from H_2O_2

A CCK-8 kit was used to evaluate whether [KER + FLA + AgNPs] could protect against the proliferation in INS-1 cells from H_2O_2. INS-1 cells were incubated with H_2O_2 containing 25.0 μmol/L of NC for 72 h. Finding, indicated that cell proliferation in the group treated with H_2O_2 was significantly higher than in the other groups treated after 72 h ($p < 0.05$). As shown in Fig. 9C, in the NC group, the proliferation of INS-1 cells was significantly ($p < 0.05$) lower (1.4 fold) than in the H_2O_2 group at 72 h.

4. Conclusions

In our investigation, we have studied a novel therapeutic approach to protect pancreatic β- cells from oxidative stress induced by H_2O_2 in INS-1 cells based on keratin powder with colloidal silver nanoparticles, denominate [KER + AgNP], enriched with flavonoids extracted from cranberry. The formulated [KER + FLA + AgNPs], physicochemical properties, releasing capacity, flavonols entrapment efficiency, and stability were evaluated by various spectral analyzers, and the results confirmed the properties of NPs. The maximum absorption (λmax) shift in UV–visible spectrophotometer

was used to identify flavonols entrapped in a keratin carrier. The physicochemical properties of formulated [KER + FL A + AgNPs] were measured by XRD, FTIR, SEM, and Zeta size analyzer. The experimental data suggested that [KER + FLA + AgNPs] show high efficiency in inhibiting ROS formation, which supports that keratin forms a coating layer over silver nanoparticles, stabilizing the [KER + FLA + AgNPs] nanocomposite. Increasing levels of CAT, SOD, GPx, GSH, stimulated cellular antioxidant defense system, which maintain an intracellular redox balance and act as free radical scavenging in hydrogen peroxide-induced oxidative stress in pancreatic β-cells. Our study supports the protective effect of KER + FLA + AgNPs, against H_2O_2-induced apoptosis and proliferatioin in INS-1 cells. These results suggest that nanocomposites could diminish H_2O_2-induced intracellular oxidant stress, either by protecting the severe depletion of antioxidant enzymes or by the direct scavenging of ROS have an important role in the preservation of β-cell physiology against oxidant stress.

Declaration of Competing Interest

None.

References

Anello, M., Lupi, R., Spampinato, D., Masini, P.M., Boggi, U., Prato, S., Rabuazzo, A.M., Purrello, F., Marchetti, P., 2005. Functional and morphological alterations of mitochondria in pancreatic beta cells from type 2 diabetic patients. Diabetologia. 48, 282–289.

Aouacheri, W., Saka, S., Djafer, R., Lefranc, G., 2009. Protective effect of diclofenac towards the oxidative stress induced by paracetamol toxicity in rats. Ann. Biol. Clin. (Paris) 67, 619–627.

Aranda, A., Sequedo, L., Tolosa, L., Quintas, G., Burello, E., Castell, J.V., Gombau, L., 2013. Dichloro- dihydro-fluorescein diacetate (DCFH-DA) assay: A quantitative method for oxidative stress assessment of nanoparticle-treated cells. Toxicol. in Vitro. 27, 954–963. https://doi.org/10.1016/j.tiv.2013.01.016.

Blois, M.S., 1960. Free Radicals in Biological Systems. Science 132, 306–307.

Brown, P.N., Turi, C.E., Shipley, P.R., Murch, S., 2012. Comparisons of large (*Vaccinium macrocarpon* Ait.) and small (*Vaccinium oxycoccos* L., *Vaccinium vitis-idaea* L.) cranberry in British Columbia by phytochemical determination, antioxidant potential, and metabolomic profiling with chemometric analysis. Planta Med. 78, 630–640. https://doi.org/10.1055/s-0031-1298239.

Drózdz, P., Šežiene, V., Wójcik, J., Pyrzyńska, K., 2017. Evaluation of bioactive compounds, minerals and antioxidant activity of Lingonberry (Vaccinium vitis-idaea L.) fruits. Molecules 23, 53. https://doi.org/10.3390/molecules23010053.

Duan, D., Wei, G., Guo, C., Cui, J., Yan, J., Yin, Y., Guan, Y., Weng, Y., Zhu, Y., Wu, X., Wang, Y., Xi, M., Wen, A., 2015. *Aralia taibaiensis* protects cardiac myocytes against high glucose-induced oxidative stress and apoptosis. Amer. J. Chinese Med 43 (6), 1159–1175.

Evans, J.L., Goldfine, I.D., Maddux, B.A., Grodsky, G.M., 2002. Oxidative stress and stress-activated signaling pathways: A unifying hypothesis of type 2 diabetes. Endocr. Rev. 23, 599–622.

Ferrier, J., Djeffal, S., Morgan, H.P., Vander Kloet, S.P., Redžić, S., Cuerrier, A., Arnason, J.T., 2012. Antiglycation activity of *Vaccinium* spp. (Ericaceae) from the Sam Vander Kloet collection for the treatment of type II diabetes. Botany. 90, 401–406. https://doi.org/10.1139/B2012-026.

Gurgul-Convey, E., Mehmeti, I., Plötz, T., Jörns, A., Lenzen, S., 2016. Sensitivity profile of the human EndoC-betaH1 beta cell line to proinflammatory cytokines. Diabetologia. 59, 2125–2133.

Howell, A.B., Botto, H., Combescure, C., Blanc-Potard, A.B., Gausa, L., Matsumoto, T., Tenke, P., Sotto, A., Lavigne, J.P., 2010. Dosage effect on uropathogenic *Escherichia coli* anti-adhesion activity in urine following consumption of cranberry powder standardized for proanthocyanidin content: a multicentric randomized double blind study. BMC Infect. Dis. 10, 94–98. https://doi.org/10.1186/1471-2334-10-94.

Jin, X., Wang, Y., Yuan, J., Shen, J., 2016. Extraction, characterization, and NO release potential of keratin from human hair. Mater. Lett. 175, 188–190. https://doi.org/10.1016/j.matlet. 2016.04.036.

Jörns, A., Mehmeti, I., Lenzenm, S., 2016. Comparative analysis of cytoprotective enzyme equipment in human pancreatic beta-cells and non-beta-cells. Diabetologia 59 suppl 1), S218.

Kappus, H., 1987. Oxidative stress in chemical toxicity. Archives Toxicol 60, 144–149.

Lenzen, S., 2008. Oxidative stress: the vulnerable beta-cell. Biochem. Soc. Trans. 36, 343–347.

Li, Y., Zhi, X., Lin, J., You, X., Yuan, J., 2017. Preparation and characterization of DOX loaded keratin nanoparticles for pH/GSH dual responsive release. Mater. Sci. Eng. C. 73, 189–197.

Liang, Y., Niu, Ma., Dan, L., Li, D., Qing Xia, W., Huang, W., 2017. Eriodictyol 7-O-β-D glucopyranoside from *Coreopsis tinctoria* Nutt. ameliorates lipid disorders via otecting mitochondrial function and suppressing lipogenesis. Mol. Med. Rep. 16, 1298–1306. https://doi.org/10.3892/mmr.2017.6743.

Liu, J., Jiao, Z., Yang, W., Zhang, C., Liu, H., Lv, Z., 2015. Variation in Phenolics, Flavanoids, antioxidant and tyrosinase inhibitory activity of peach blossoms at different developmental stages. Molecules. 20, 20460–20472. https://doi.org/10.3390/molecules201119709.

Lyu, G., Wang, Y., Huang, X., Zhang, H., Sun, L., Liu, Y., Yan, C., 2016. Hydrophilic CeO_2 nanocubes protect pancreatic β-cell line INS-1 from H_2O_2-induced oxidative stress. Nanoscale. 8, 7923–7932.

Marinho, H.S., Cyrne, L., Cadenas, E., Antunes, F., 2013. H2O2 delivery to cells: steady-state versus bolus addition. Methods Enzymol. 526, 159–173.

Martin, J.J., Cardamone, J.M., Irwin, P.L., Brown, E.M., 2011. Keratin capped silver nanoparticles – Synthesis and characterization of a nanomaterial with desirable handling properties. Colloids Surf. B: Biointerfaces. 88, 354–361. https://doi.org/10.1016/j.colsurfb.2011.07.013.

Nel, A., 2006. Toxic Potential of Materials at the Nanolevel. Science 311, 622–627. https://doi.org/10.1126/science.1114397.

Nikki, K.E., 2001. Free Radical in the 1990s from *in Vitro* to *in Vivo*. Free Rad. Res. 33, 693–704.

Peixoto, T.C., Moura, E.G., Oliveira, E., Soares, P. N., Guarda, D. S., Bernardino, D. N., Lisboa, P.C. 2017. Cranberry (Vaccinium macrocarpon) extract treatment improves triglyceridemia, liver cholesterol, liver steatosis, oxidative damage and corticosteronemia in rats rendered obese by high fat diet. Eur. J. Nutr, DOI 10.1007/s00394-017-1467-2.

Pi, J., Zhang, Q., Fu, J., Woods, C.G., Hou, Y., Corkey, B.E., Collins, S., Andersen, M.E., 2010. ROS signaling, oxidative stress and Nrf2 in pancreatic beta-cell function. Toxicol. Appl. Pharmacol 244, 77–83.

Shu, Y.Z., 1998. Recent natural products based drug development: A pharmaceutical industry perspective. J. Nat. Prod. 61, 1053–1071.

Skarpańska, A., Trzeciak, J., Michalska, A., Kafkas, M.E., Woitas-Ślubowska, D., 2017. Effects of cranberry (*Vaccinum macrocarpon*) supplementation on iron status and inflammatory markers in rowers. J. Intern. Soc. Sports Nutr 14, 7–16. https://doi.org/10.1186/s 12970-017- 0165-z.

Slimen, I.B., Najar, T., Ghram, A., Dabbebi, H., Ben-Mrad, M., Abdrabbah, M., 2014. Reactive oxygen species, heat stress and

oxidative-induced mitochondrial damage. A review. Int. J. Hyperthermia. 30, 513–523.

Stancill, J.S., Broniowska, K.A., Oleson, B.J., Naatz, A., John, A.C., 2019. Pancreatic-cells detoxify H2O2 through the peroxiredoxin/thioredoxin antioxidant system. J. Biol. Chem. 294, 4843–4853. https://doi.org/10.1074/jbc.RA118.006219.

Suman, T.Y., Rajasree, S.R., Kanchana, A., Elizabeth, S.B., 2013. Biosynthesis, characterization and cytotoxic effect of plant mediated silver nanoparticles using *Morinda citrifolia* root extract. Colloids Surf B Biointerf. 106, 74–78. https://doi.org/10.1016/j.colsurfb.2013.01.037.

Sun, B., Sun, G.B., Xiao, J., Chen, R.C., Wang, X., Wu .Y, 2012. Isorhamnetin inhibits H2O2-induced activation of the intrinsic apoptotic pathway in H9c2 cardiomyocytes through scavenging reactive oxygen species and ERK inactivation. J. Cell Biochem, 113, 473–85.

Sun, J., Liu, W., Ma, H., Marais, J.P.J., Khoo, C., Dain, J.A., Seeram, N.P., 2016. Effect of cranberry *(Vaccinium macrocarpo*n) oligosaccharides on the formation of advanced glycation end-products. J. Berry Res. 6, 149–158. https://doi.org/10.3233/JBR-160126.

Stefanescu (Braic), R., Vari, C., Imre, S., Huţanu, A., Fogarasi, E., Todea, T., Dogaru, M., 2018. Vaccinium Extracts as modulators in experimental type 1 diabetes. J. Med. Food, 21, 1106-1112. doi: 10.1089/jmf.2017.0141.

Supale, S., Li, N., Brun, T., Maechler, B., 2012. Mitochondrial dysfunction in pancreatic b cells. Trends Endocrinol. Metab 23, 477–487.

Tamerler, C., Oren, E.E., Duma, M., Venkatasubramanian, E., Sarikay, M., 2006. Adsorption kinetics of an engineered gold binding peptide by surface plasmon resonance spectroscopy and a quartz crystal microbalance. Langmuir 2, 7712–7718.

Templeton, A.C., Wuelfing, W.P., Murray, R.W., 2000. Monolayer-protected cluster molecules. AccChem. Res. 33, 27–36.

Valko, M., Leibfritz, D., Moncol, J., Cronin, M.T.D., Mazur, M., Telser, j., 2007. Free radicals and antioxidants in normal physiological functions and human disease. Int. J. Biochem. Cell. Biol. 39,44– 84.

Vvedenskaya, I.O., Rosen, R.T., Guido, J.E., Russell, D.J., Mills, K. A., Vorsa, N., 2004. Characterization of flavonols in cranberry (Vaccinium macrocarpon) powder. J. Agric. Food Chem. 52, 188–195. https://doi.org/10.1021/jf034970s.

Wang, Q., Wu, J., Wang, W., Wang, A., 2011. Preparation, Characterization and Drug-Release Behaviors of Crosslinked Chitosan/Attapulgite Hybrid Microspheres by a Facile Spray-Drying Technique. J. Biomater. Nanobiotechnol. 2, 250–257. https://doi.org/10.4236/jbnb.2011.23032.

Wang, L., Wu, Y., Xie, J., Wang, L., Wu, Y., Xie, J., Wu, S., Wu, Z., 2018. Characterization, antioxidant and antimicrobial activities of green synthesized silver nanoparticles from *Psidium guajava* L. leaf aqueous extracts. Mater Sci Eng C 86, 1–8.

Xu, Q., Chen, S.Y., Deng, L.D., Feng, L.P., Huang, L.Z., Yu, R.R., 2013. Antioxidant effect of mogrosides against oxidative stress induced by palmitic acid in mouse insulinoma NIT-1 cells. Brazilian J. Med. Biol. Res 46, 949–955. https://doi.org/10.1590/1414-431X20133163.

Yagi, K., 1998. Simple procedure for specific assay of lipid hydroperoxides in serum or plasma. Methods Mol. Biol 108, 07–110.

Zhang, Q., Hu, C., Yan, K., 2015. Preparation and characterization of silver nanoparticles from the super-heated water degraded keratin solutions. J. Nanosci. Nanotechnol. 15, 6790–6797.

Zheng, W., Wang, S.Y., 2003. Oxygen radical absorbing capacity of phenolics in blueberries, cranberries, chokeberries, and lingonberries. J. Agric. Food. Chem. 51, 502–509.

Zhong, Z., Patskovsky, S., Bouvrette, P., 2004. the surface chemistry of au colloids and their interactions with functional amino acids. J. Phys. Chem. B. 108, 4046–4049.

Zhu, M., Wu, W., Jiao, L., Yang, P., Guo, M., 2015. Analysis of flavonoids in lotus (*Nelumbo nucifera*) leaves and their antioxidant activity using macroporous resin chromatography coupled with LC- MS/MS and antioxidant biochemical assays. Molecules. 20, 10553–10565. https://doi.org/10.3390/molecules200610553.

Zucca, P., Rosa, A., Tuberoso, C.I.G., Piras, A., Rinaldi, A.C., Sanjust, E., Dessì, M.A., Rescigno, A., 2013. Evaluation of antioxidant potential of "Maltese Mushroom" (*Cynomorium coccineum)* by means of multiple chemical and biological assays. Nutrients. 5, 149–161. https://doi.org/10.3390/nu5010149.